Journal of Nanobiotechnology

RESEARCH Open Access

Targeting phosphatidylserine in tumor cell membranes with a zinc-containing molecule to efficiently combat tumor metastasis

Xiao-Hong Zhou[1,4†], Jia-Wei Wang[3†], Wei You[4], Fan Gao[4], Zhe Wang[4], Hong-Jie Gao[4], Ai-Zong Shen[1,6], Yang-Huan Ou[2*], Xiang Zhan[5*], Xuan Nie[1,6*], Li-Qin Tang[1,6*] and Ye-Zi You[1,4*]

Abstract

Metal drugs, such as platinum drugs, are widely used in tumor treatment. However, most traditional tumor treatments face the risk of failure due to the ineffective control over drug resistance and tumor metastasis. Targeting the cell membrane and disrupting its function to combat drug resistance and metastasis is a promising strategy. Nevertheless, membranolytic drugs always cause significant cytotoxicity. In this study, we developed a zinc-containing molecule to selectively kill tumor cells by targeting phosphatidylserine in the tumor cell membrane, which is commonly distributed in the outer cell membrane of tumor cells. Herein, a structurally optimized amphiphilic zinc-containing molecule, 2aZn, was developed by screening the appropriate hydrophobic tail and linker. This functional molecule can disrupt the tumor cell membrane to kill various types of tumor cells with minimal damage to normal tissue. After repeated stimulation, no obvious drug resistance was observed. Importantly, 2aZn could successfully combat tumor metastasis by destroying the cell membrane and reducing the capacity of cells to invade. As a result, zinc-containing molecules have the potential to overcome drug resistance and tumor metastasis in the treatment of tumors, providing a new perspective for the design of effective antitumour medications.

†Xiao-Hong Zhou and Jia-Wei Wang contributed equally to this work.

*Correspondence:
Yang-Huan Ou
auyeungfoon1010@ahmu.edu.cn
Xiang Zhan
zhanxiang@ahmu.edu.cn
Xuan Nie
niexuan@ustc.edu.cn
Li-Qin Tang
tangliqin@ustc.edu.cn
Ye-Zi You
yzyou@ustc.edu.cn

Full list of author information is available at the end of the article

Graphical Abstract

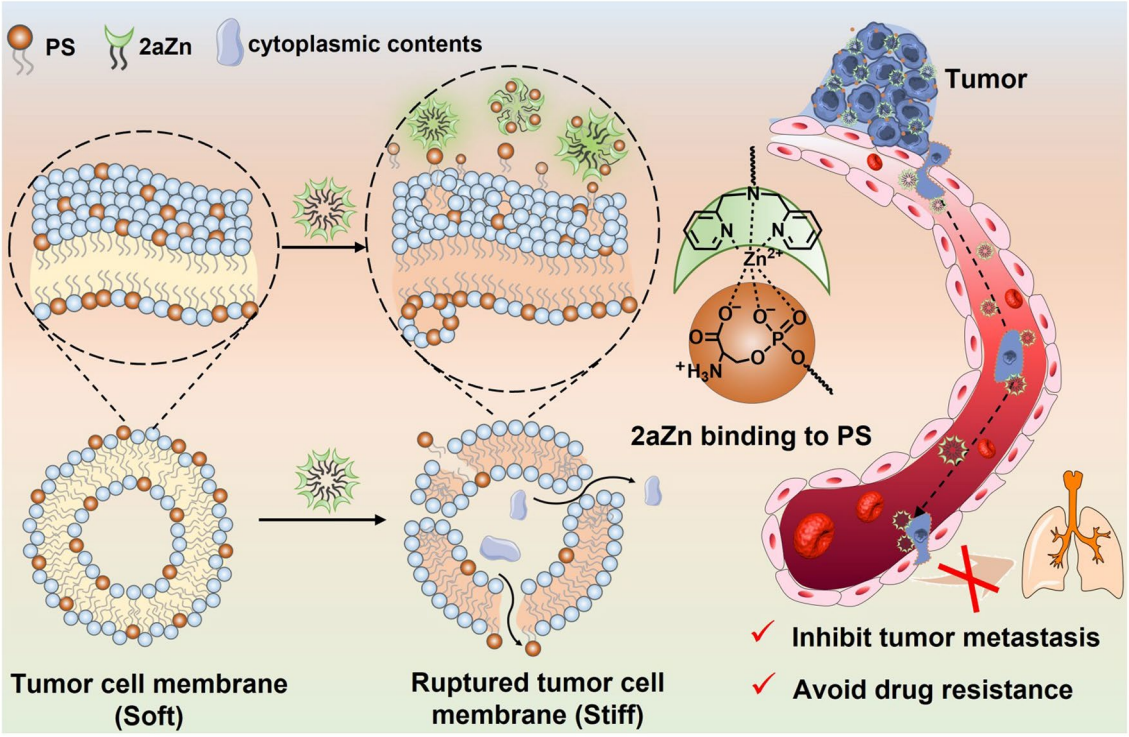

Keywords Antitumour drug, Tumor targeting, Phosphatidylserine, Cell membrane disruption, Tumor metastasis inhibition, Overcoming drug resistance

Introduction

Despite significant advances in cancer treatment over the past decades [1], malignancies remain a persistent global health challenge [2, 3]. Chemotherapy remains a cornerstone in clinical cancer treatment [4]. However, several drawbacks limit the application of chemical agents, such as poor bioavailability and a lack of tumor-targeting ability, thereby leading to systemic toxicity [5–7]. In addition, with the progression of cancer, many patients who are receiving chemotherapy exhibit drug resistance and tumor metastasis [8, 9]. Although many innovative tumor treatment strategies have emerged, many are too complicated and not conducive to clinical translation [10–12]. Therefore, devising a straightforward yet potent strategy for tumor treatment with enhanced selectivity while circumventing drug resistance and metastasis is imperative.

Within biological systems, the cell membrane governs material exchange and cellular activities [13]. It is a crucial barrier for antitumour drugs that need to enter cells to exert their effects [14, 15]. Thus, disrupting tumor cell membranes can increase the internalization of clinical drugs [16, 17]. Moreover, owing to the low mutation of cell membranes and their essential role in cell migration, the disruption of cell membranes can minimize drug resistance development while inhibiting tumor metastasis [18, 19]. Several achievements have been made in the selective destruction of tumor cell membranes to eliminate tumors on the basis of unique tumor microenvironments, particularly acidic environments [20–23]. For example, Wang and his collaborators developed a pH-sensitive nanodetergent that can specifically disrupt tumor cell membranes in an acidic tumor environment to cause direct death of tumor cells without harming normal cells [21]. Xiong et al. developed a strategy to develop oncolytic polymers with a precise structure for selective oncolytic therapy, which could switch the membranolytic activity within 0.2 pH units [22]. Despite these achievements, highly selective disruption of tumor cell membranes remains a challenge. Phosphatidylserine (PS) is a kind of phospholipid present in the outer leaflet of tumor cell membranes but is absent from the outer leaflet of normal cells [24, 25]; it regulates tumorigenesis, metastasis, and immune evasion [26, 27]. Therefore, PS is a robust therapeutic target in tumors. PS-targeting strategies, such as PS-binding antibodies (e.g., bavituximab) and Annexin V-derived peptides, have demonstrated

antitumour effects [24]. However, the clinical translation of these biomacromolecular drugs is hindered by poor stability, high cost, and limited tissue penetration. Moreover, these agents still rely on the activation of diverse signalling pathways to induce tumor cell death, rendering them incapable of circumventing the development of drug resistance. Therefore, developing small-molecule agents capable of highly selective disruption of tumor cell membranes through strong PS recognition holds significant promise for achieving drug resistance evasion, metastasis suppression, and clinical translation in cancer treatment.

Unlike traditional platinum-based therapies (e.g., cisplatin and oxaliplatin) that target DNA, some other metal complexes can improve tumor selectivity and overcome some resistance through unique mechanisms, such as targeting tumor-specific biomarkers, disrupting tumor cell homeostasis, activating immune responses, and inducing nonapoptotic death [28]. Metal complexes formed from ligands such as dipicolylamine (DPA) and terpyridine, especially zinc-dipicolylamine, have been widely used as functional recognition motifs in the design of PS-targeted apoptosis probes and immunotherapeutic molecules because of their ability to specifically bind to PS [29, 30]. However, few studies have developed drugs based on such structures that can accurately recognize PS and directly kill cancer cells via a membrane lysis mechanism. Moreover, the application potential of these drugs in overcoming drug resistance and inhibiting tumor metastasis remains unexplored.

In this study, we constructed a library of amphiphilic metal complexes based on DPA to achieve efficient cancer therapy while circumventing drug resistance and metastasis. Cytotoxicity screening revealed a DPA-Zn-based complex, 2aZn, with potent antitumour efficacy and high selectivity. Owing to its amphiphilic nature, 2aZn self-assembles into stable nanoparticles. Its DPA-Zn headgroup specifically recognizes PS on the outer leaflet of tumor cell membranes, enabling selective accumulation in tumor tissues (Fig. 1). Subsequently, 2aZn disrupts membrane stability through electrostatic and hydrophobic interactions, inducing membrane rupture and tumor cell death. Notably, the reduced fluidity of damaged membranes restricts cellular motility, thereby inhibiting tumor cell invasion. Unlike platinum-based therapies that target DNA, 2aZn employs a unique

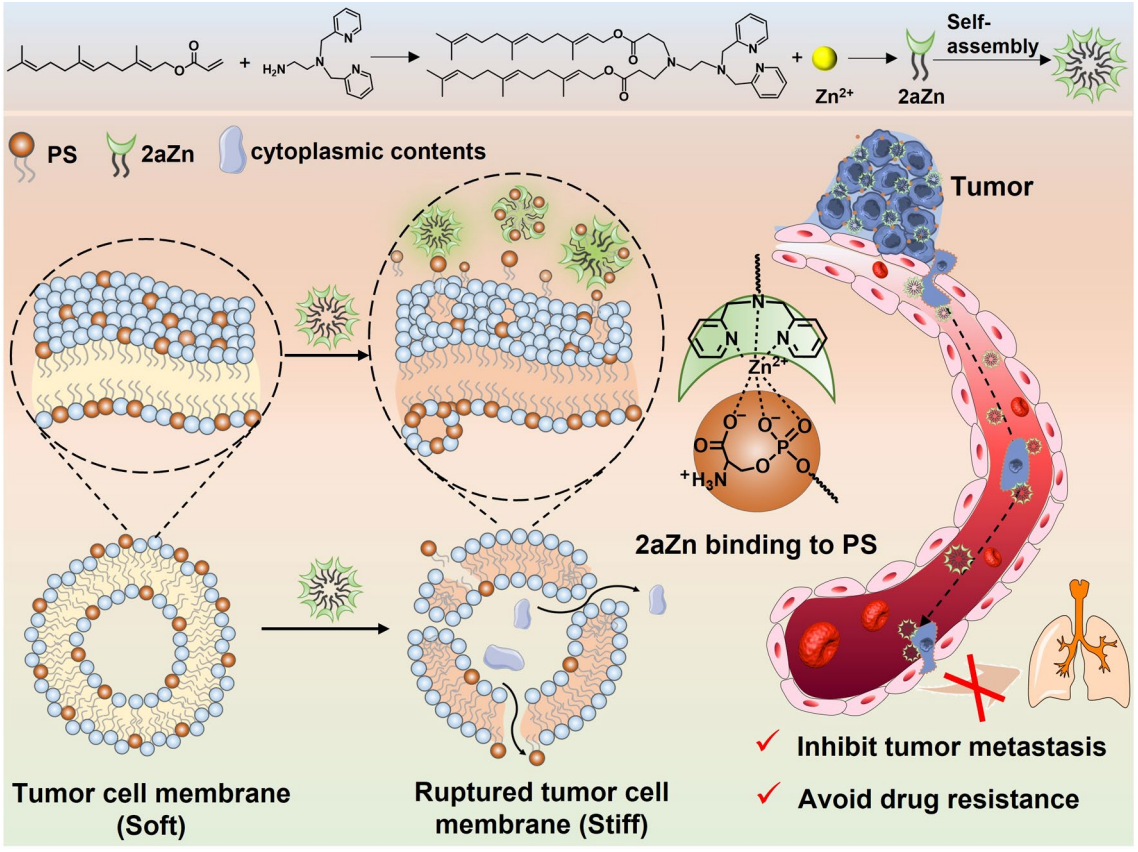

Fig. 1 Scheme of the phosphatidylserine-targeted strategy to destroy the tumor cell membrane to combat tumor metastasis. The amphiphilic Zn complex 2aZn selectively binds to PS on the outer leaflet of tumor cell membranes, leading to membrane disruption and stiffening. This process facilitates the selective elimination of tumor cells without inducing drug resistance and effectively inhibits tumor metastasis

membrane-targeting destruction mechanism to eliminate tumor cells, effectively overcome drug resistance. Both in vitro and in vivo experiments have demonstrated the significant therapeutic potential of this strategy. Consequently, this tumor cell membrane destruction induced by targeting PS in the membrane of tumor cells holds great promise for overcoming tumor drug resistance and inhibiting tumor metastasis.

Experimental section

Reagents

All reagents were used as received from commercial sources unless otherwise stated. All reagents used for chemical synthesis, including 2,2'-dipicolylamine (DPA, 98%), tert-butyl N-(2-bromoethyl) carbamate (98%), N-(tert-butoxycarbonyl)tyramine (98%), acrylate (98%), oleyl alcohol (90%), farnesol (98%), hexadecanol (98%), dodecanol (98%), acryloyl chloride (98%), $Zn(NO_3)_2$ (98%), $Co(NO_3)_2$ (98%), and $Ni(NO_3)_2$ (98%), were purchased from Sigma. Other reagents used for chemical synthesis were purchased from Sinopharm Chemical Reagent Co., Ltd. The methylthiazolyldiphenyl-tetrazolium bromide (MTT), calcein-AM fluorescence probe, and other kits were purchased from Thermo Fisher Scientific.

General characterization

^1H NMR spectra were characterized on a Bruker AC-400FT spectrometer (400 MHz). The MTT results were recorded on a Thermo Varioskan flash spectral scanning multimode reader. The zeta potential and hydrodynamic diameter of the nanoparticles were characterized with a NanoBrook 90Plus PALS. Transmission electron microscopy (TEM) images were obtained from a Hitachi Model H-7650 transmission electron microscope with an accelerating voltage of 100 kV. Scanning electron microscopy (SEM) images were obtained from a GeminiSEM 500 field emission scanning electron microscope. All the fluorescence images were taken with an Olympus IX71 microscope. Confocal images were obtained via a ZEISS LSM 980 confocal laser scanning microscope. Flow cytometric analysis was performed with a Beckman Cytoflex flow cytometer. The Zn ion content was measured via a Thermo Fisher iCAP RQ inductively coupled plasma spectrometer (ICP-MS).

Cell lines and cell culture

The human embryonic kidney cell line (293T) was purchased from ATCC. The murine embryonic fibroblast cell line (3T3), murine macrophage cell line (RAW 264.7), human cervical carcinoma cell line (HeLa), human glioblastoma cell line (U373), murine colon carcinoma cell line (CT-26), human liver cancer cell line (HepG2), murine mammary adenocarcinoma cell line (4T1), 4T1 cell line stably expressing luciferase (Luc-4T1), and DOX-resistant human breast carcinoma cell line (MCF-7/ADR) were purchased from Procell (Wuhan, China). HeLa and U373 cells were cultured in DMEM with 10% FBS and 1% penicillin/streptomycin solution. The other cells were cultured in RPMI 1640 medium supplemented with 10% FBS and 1% penicillin/streptomycin solution. MCF-7/ADR cells were cultured in complete RPMI 1640 medium supplemented with 0.5 mg/mL DOX to maintain drug resistance. All the cells were cultured in a humidified incubator at 37 °C in a 5% CO_2 atmosphere.

Synthesis of linker a

Linker a of the amphiphilic metal complexes was synthesized via the following steps: tert-butyl N-(2-bromoethyl) carbamate (1.78 g, 8.0 mmol) and DPA (1.59 g, 8.0 mmol) were dissolved in 30.0 mL of acetonitrile. Afterward, anhydrous K_2CO_3 (5.52 g, 40 mmol) was added to the reaction mixture. The reaction was maintained at 80 °C for 24 h under a N_2 atmosphere. After the reaction was complete, the mixture was filtered, and the filtrate was collected. The crude product was purified by silica gel column chromatography using ethyl acetate/methanol (7:1, V/V) as the eluent, affording the Boc-protected amine intermediate. The intermediate was dissolved in a mixture of trifluoroacetic acid and DCM (1:4, V/V) and allowed to react overnight. Then, sodium hydroxide was applied to adjust the pH to 12. The solution was extracted with dichloromethane (20.0 mL × 3), and the organic phase was collected and dried over anhydrous Na_2SO_4. Finally, the solvent was removed by rotary evaporation to obtain product a (1.0 g, 52% yield). The ^1H NMR spectrum of linker a is shown in Fig. S1.

Synthesis of linker B

Linker b of the amphiphilic metal complexes was synthesized as follows: DPA (3.00 g, 15 mmol), paraformaldehyde (0.47 g), and hydrochloric acid (0.5 mL) were added to MeOH (25 mL) and heated to reflux. When the mixture became a clear yellow solution, N-(tert-butoxycarbonyl) tyramine (4.55 g, 13 mmol) was added, and the mixture was refluxed for another 4 days. The solvent was removed by rotary evaporation, and the crude product was purified by a silica gel column with DCM/MeOH (10:1, V/V). The obtained Boc-protected amine intermediate was dissolved in a mixture of trifluoroacetic acid and DCM (1:4, V/V) to react overnight. The solvent was removed by rotary evaporation, and then sodium hydroxide was applied to adjust the pH to 12. The solution was extracted with dichloromethane (20.0 mL × 3), and the organic phase was collected and dried over anhydrous Na_2SO_4. Finally, the solvent was removed by rotary evaporation to obtain product b (3.66 g, 70% yield). The ^1H NMR spectrum of linker b is shown in Fig. S2.

Synthesis of amphiphilic metal complexes

To synthesize amphiphilic metal complexes, the hydrophobic tail was first prepared. For example, hydrophobic tail 2 was synthesized as follows: farnesol (2.22 g, 1.0 mmol) and trimethylamine (1.01 g, 1.0 mmol) were added to 50.0 mL anhydrous DCM. Then, acryloyl chloride (0.95 g, 1.0 mmol in 10 mL DCM) was added dropwise to the mixture at 0 °C. The mixture was stirred at room temperature for 12 h under a N_2 atmosphere. Triethylamine hydrochloride was removed by filtering and washing three times with water. Finally, the organic phase was concentrated and dried to obtain a hydrophobic tail 2 (2.48 g, 90% yield). Next, linker a (0.97 g, 0.4 mmol) and hydrophobic tail (2.76 g, 1.0 mmol) were added to 5.0 mL of DMF in a tube. The air was removed from the tube, and it was sealed. The mixture was maintained at room temperature for 48 h at 90 °C. Then, silica gel column purification was performed with DCM/MeOH (10:1, V/V) elution to obtain the desired product (1.52 g, 48% yield). Finally, the product was reacted with $Zn(NO_3)_2$ (1.0 equiv) in MeOH for 4 h at room temperature to obtain the desired product, which was labelled as 2aZn. Other amphiphilic metal complexes were synthesized through similar methods. The ^1H NMR spectra of the synthesized molecules are shown in Fig. S3 to Fig. S16.

In vitro cytotoxicity test

In vitro cytotoxicity was evaluated via the MTT assay. The cells were plated in 96-well plates (5,000 cells/well). After incubation for 24 h, the cells were incubated with different molecules at specific concentrations for 24 h. The medium was replaced with fresh medium containing MTT. After incubation for another 4 h, the resulting formazan crystals were dissolved in 100 μL of DMSO. The absorbance (A) of the solution in each well was detected at 492 nm by a microplate reader. Cell viability (%) = $A_{(sample)}/A_{(PBS)} \times 100\%$. $A_{(sample)}$ represents the absorbance of the tested compound group, and $A_{(PBS)}$ represents the absorbance of the PBS group.

Hemolysis test

The toxicity of 2aZn to mammalian erythrocytes was investigated using fresh rat red blood cells (RBCs). Briefly, fresh blood was extracted from the orbital venous plexus of each mouse. Following centrifugation and several washes with PBS, the RBCs were subsequently isolated. An RBC suspension was obtained by diluting (25-fold) with PBS to achieve 4% (V/V) RBC content (containing 10% FBS). 2aZn was dissolved in saline at different concentrations. Seventy-five microlitres of 2aZn solution was then mixed with 225 μL of the diluted RBC suspension, and the RBC suspension treated with Triton was used as the control. The mixtures were then incubated at 37 °C for 1 h. After that, the mixture was subjected to centrifugation (1,000 × g for 5 min, 4 °C), and 100 μL aliquots of the supernatant were pipetted into a 96-well microplate. The released hemoglobin was measured spectrophotometrically by measuring the absorbance of the samples at 576 nm via a microplate reader.

Scanning electron microscopy assay

CT-26 cells were seeded in 6-well plates (8×10^5 cells/well) with a cover slip at the bottom of each well. After incubation for 24 h, the cells were washed with PBS and subsequently incubated with 2aZn at the IC_{50} in complete medium for 1 h. After incubation, the supernatant was removed, and the cells were washed twice with PBS. The remaining adherent cells were fixed after a 4-hour incubation at 4 °C with PBS containing 2.5% glutaraldehyde. Next, the samples were washed three times with PBS and dehydrated via a series of ethanol solutions (10%, 30%, 50%, 70%, 90%, 100%). After the alcohol evaporated, the sample was observed via SEM.

Calcein-AM/PI double-staining assay

HeLa cells were seeded onto a 24-well plate and allowed to incubate overnight. The cell culture medium was then removed and replaced with fresh medium containing 2aZn at different concentrations. After 24 h of incubation, the cells were washed three times with PBS and subsequently stained with calcein-AM and propidium iodide (PI) dyes according to the manufacturer's instructions. The cells were then observed under a fluorescence microscope.

Annexin V-FITC/PI assay

HeLa cells were seeded in 12-well plates (1.0×10^5 cells/well). After 24 h of incubation at 37 °C, the cells were treated with 2aZn (10 μM, 30 μM) for 24 h. The cells were harvested and collected via trypsinization and then centrifuged at 1000 × g for 5 min and washed twice with cold PBS. Finally, the cells were stained with both Annexin V-FITC and PI dyes according to the manufacturer's protocol. The fluorescence was analysed by flow cytometry.

ATP release assay

A total of 8.0×10^5 HeLa cells were seeded into a 12-well plate and cultured for 24 h. Then, the medium was replaced with fresh medium containing varying concentrations of 2aZn. Following 4 h of incubation, the culture medium (1.0 mL) was collected, and the debris from the cells was completely removed by centrifugation for 10 min. Next, the ATP content in the medium was measured with a chemiluminescence ATP determination kit according to the manufacturer's manual.

LDH release assay

HeLa cells were seeded in 96-well plates (5×10^3 cells/well) in 100 μL of medium. After the cells were incubated for 24 h, the medium was replaced with fresh medium containing various concentrations of 2aZn. Following 4 h of incubation, the supernatant was centrifuged at 400 × g for 5 min. LDH levels were determined via an LDH test kit according to the manufacturer's protocol.

The liposome leakage and fluidity evaluation

Phospholipids were dissolved in a chloroform and methanol mixture (2:1, V/V). Lipids (0.5 μmol in total) with the indicated compositions were mixed in a glass vial. The solvent was removed under a stream of nitrogen, and the lipid film was dried in a vacuum environment for 30 min. Then, the film was hydrated at room temperature with 500 μL of buffer (20 mM HEPES, 150 mM NaCl, pH = 7.5) containing 50 mM 5(6)-carboxyfluorescein (Sigma). Finally, the liposomes were obtained by extrusion of the hydrated lipids through a polycarbonate filter (Whatman, 100 nm) 22 times with a Mini-Extruder device (Avanti Polar Lipids Inc.). The free 5(6)-carboxyfluorescein was removed by desalting columns (7000 MWCO). After treatment with different concentrations of 2aZn, the fluorescence of the mixture was monitored with a Thermo Scientific Microplate Reader (excitation: 485 nm, emission: 510 nm). The zeta potential and morphology of the liposomes after treatment with 2aZn (20 μM) were observed with a zeta potential detector and TEM, respectively. For the evaluation of membrane fluidity. Liposomes with the indicated compositions were prepared via the same method. Then, TMA-DPH (Thermo Fisher) was used to evaluate the membrane fluidity of the liposomes after treatment with 2aZn according to previous methods.

Giant vesicle preparation and Annexin V-FITC/FM4-64 staining assay

First, a lipid stock solution (1.0 mg/mL) was prepared in DCM and MeOH mixed solvent (2:1 V/V). A drop of stock lipid mixture (1.0 mL) was added to a beaker made of Teflon. Thereafter, the solvents were removed at room temperature, and the beaker was placed under vacuum for 2 h. Finally, the giant vesicles were obtained by hydrating the lipid film with warm (50 °C) water (the final concentration of lipid was 500 μM). The prepared giant vesicles were subsequently incubated with 2aZn. Then, the giant vesicles were stained with both Annexin V-FITC and FM4-64 dyes. Finally, the giant vesicles were observed via a confocal laser scanning microscope.

Drug resistance development evaluation

Drug resistance development was evaluated following a previously published method [19]. In brief, HepG2 cells were exposed to 2aZn (20 μM) or oxaliplatin (100 nM) for increasing durations, ranging from 1 h to 24 h (1, 2, 4, 12, 24 h). After a single exposure, the cells were digested to grow for the next treatment. Each exposure time was repeated 3 times and recorded as one pulse treatment, and the pulse treatments of five times were marked as P1 to P5 generations. After each pulse treatment, the cytotoxicity of 2aZn and oxaliplatin to the treated cells was measured.

Cytotoxicity in multidrug-resistant cells

The cytotoxicity of 2aZn or DOX in multidrug-resistant cells was studied via an MTT assay. MCF-7/ADR cells were seeded in 96-well plates (5×10^3 cells/well). After 24 h of incubation, the culture medium was replaced with fresh media containing various concentrations of DOX ranging from 50 to 400 μg/mL or containing both 20 μM 2aZn and various concentrations of DOX ranging from 0 to 50 μg/mL. After 48 h of incubation, the medium was replaced with 100 μL of fresh medium containing 20 μL of MTT solution (5.0 mg/mL in PBS), and the cells were cultured for 4 h. The MTT-containing medium was replaced with 150 μL of DMSO. The absorbance of the solution at 490 nm in each well was determined via a microplate spectrophotometer.

Cell migration study

HepG2 cells were seeded in 6-well plates at a density of 5×10^5 cells per well. When the cells reached 90% confluence, a scratch was made with a 200 μL pipette tip. The floating cells were rinsed off with PBS. Then, fresh medium (1% FBS) containing 2aZn (1/2 IC_{50}) or oxaliplatin (1/2 IC_{50}) was added to the cells. The cells were then incubated for 24 h. Phase contrast images of the gaps were taken via a microscope at 0 h and 24 h after scratching.

Cell adhesion experiment

HepG2 cells were seeded in 24-well plates (1×10^5 cells/well). After 24 h of incubation, the culture medium was replaced with fresh media containing various samples (PBS, oxaliplatin, and 2aZn at a concentration of 1/2 the IC_{50}). After 24 h of incubation, the cells were digested and dispersed in PBS and then seeded into another 96-well plate modified with fibronectin (FN, 10 μg/mL, Solarbio) at a density of 8×10^4 cells per well. Then, PBS was used to remove the nonadherent cells. Finally, the number of cells adhering to fibronectin was observed via a microscope.

Transwell assay

A Transwell method was used to evaluate the invasive activity of the tumor cells (HepG2 cells). Transwell (12-well) membrane filters (8.0 μm) were precoated with

Matrigel (BD Biosciences) before cell culture. One hour later, a 1 mL cell suspension (5×10^5 cells/mL) in medium without FBS was added to the top chamber of the transwells, which were subsequently cultured with different test compounds. At the same time, medium containing 10% FBS was added to the lower chamber. After 12 h of incubation, 4% paraformaldehyde was used to fix the invading cells on the lower membrane surface, after which they were stained with 0.1% crystal violet for 10 min. Finally, images were taken under a fluorescence microscope.

3D cell model

A total of 50 μL/well of hot agarose (Sigma, low-EEO) solution (0.5 wt%, dissolved in serum-free medium) was added to a 96-well plate. The samples were placed in a biosafety cabinet to cool for 1 h, after which they were sterilized with ultraviolet light. Then, 4T1 cells (1×10^3 cells/well) were seeded. 4T1 cell multicellular spheroids were harvested after approximately 3 days of growth. The culture medium was carefully replaced with fresh medium containing free DOX (0.25 μg/mL) or containing both 40 μM 2aZn and DOX (0.25 μg/mL). After 24 h of incubation, the medium was carefully removed, and the cell spheroids were gently washed with PBS. The distribution of DOX in the cell spheroids after treatment was determined via confocal laser scanning microscopy.

In vivo biodistribution

The manuscript describes all the animal experiments that were carried out following the ethical principles and directives set by the Laboratory Animal Management Committee at the University of Science and Technology of China, with the specific approval number USTCACUC23030122089. A total of 1.0×10^5 4T1 cells in 0.1 mL of PBS were injected subcutaneously into the right flank of the BALB/c mice (5 weeks old). When the tumor size reached approximately 100 mm^3, the mice were intravenously injected with 100 μL of 2aZn (10 mg/kg). Six hours, 12 h, or 24 h later, the mice were sacrificed, and the hearts, livers, spleens, lungs, kidneys, and tumors were collected. The biodistribution of 2aZn was calculated on the basis of the Zn content. The samples were freeze-dried and then digested with concentrated nitric acid at 80 °C for one day to obtain clear solutions. Ultrapure water was added to dilute the solution, and the Zn concentration was measured via ICP-MS.

In vivo antitumor activity

A total of 1.0×10^5 4T1 cells in 0.1 mL of PBS were injected subcutaneously into the mammary fat pads of the BALB/c mice (5 weeks old). When the tumors grew to 100 mm^3 (10 days postinjection), the mice were randomly divided into 3 groups, and each group contained 5 mice. The mice in each group were treated with PBS, 2aZn (10.0 mg/kg), or oxaliplatin (10.0 mg/kg) on the 1st, 3rd, or 5th day after the beginning of treatment via intratumoral injection. The width and length of the tumors in each group were measured every 2 days, and the tumor volume was calculated via the following formula: tumor volume = 1/2 × length × $width^2$. After the mice were sacrificed, the tumor tissues and organs were separated and weighed. Then, the samples were fixed in Bouin solution and stained with hematoxylin and eosin (H&E), a TUNEL staining agent, to evaluate their antitumour activity and biocompatibility.

The therapeutic effects of 2aZn in a metastasis model

A lung metastatic breast cancer model in BALB/c mice was established to investigate the therapeutic effect on metastatic cancer. Briefly, each mouse was injected intravenously with 5.0×10^5 Luc-4T1 cells and divided randomly into three groups, with five mice in each group. One day later, PBS, oxaliplatin (100 μL, 2.5 mg/mL), or 2aZn (100 μL, 2.5 mg/mL) was injected intravenously into each group every other day for a total of three times. On the 3rd, 6th, 12th, and 21st days post-treatment, the growth of pulmonary metastatic tumors was monitored via the IVIS Spectrum imaging system after injection of D-luciferin (30 mg/kg, 100 μL). At the end of monitoring, the mice were sacrificed, and the lung tissues were fixed in Bouin's solution and analysed via H&E staining.

Statistical analysis

The statistical analysis was performed with GraphPad Prism software. The data are expressed as the means ± SDs. Statistical differences between the two groups were analysed via Student's t-test. Differences were considered statistically significant at $^{*}P < 0.05$, $^{**}P < 0.01$, and $^{***}P < 0.001$.

Results and discussion

Many studies have reported that, unlike normal cells, the outer leaflet of tumor cells contains PS, making it a potential target for tumor therapy. To screen small molecules capable of selectively disrupting tumor cell membranes, we constructed a library of amphiphilic metal complexes on the basis of the structural characteristics of cationic amphiphilic anticancer peptides that disrupt cell membranes, as illustrated in Fig. 2a. Previous reports indicate that hydrophobic tails, linkers, and hydrophilic heads are pivotal in determining the properties of amphiphilic molecules [31]. Accordingly, to obtain the desired molecule, five alkyl chains with varying lengths and degrees of unsaturation, two distinct linkers, and three metal cations, Zn^{2+}, Co^{2+}, and Ni^{2+}, were used to construct a molecular library comprising 30 amphiphilic metal complexes via Michael addition reactions (synthesis

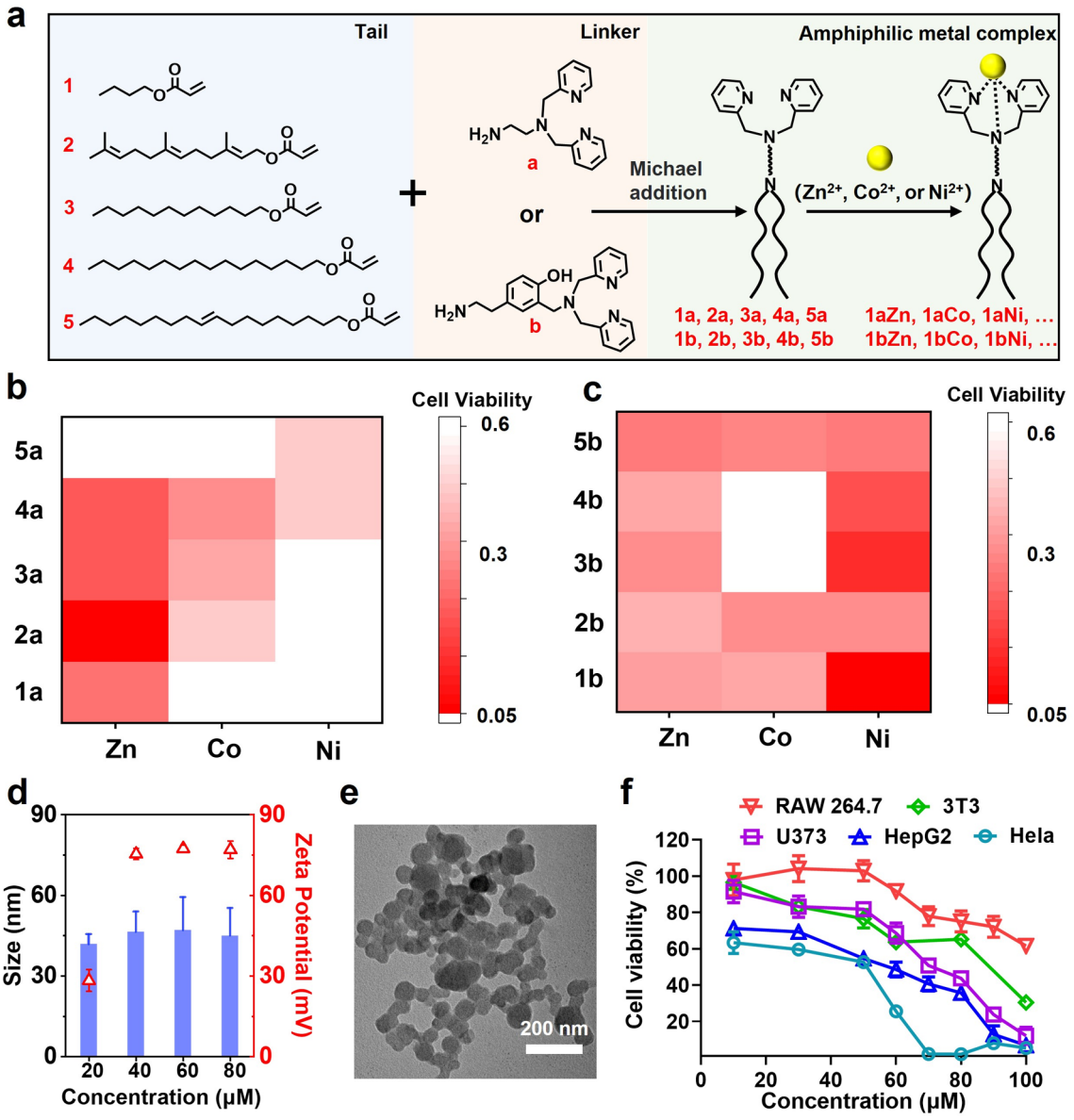

Fig. 2 Preparation, characterization, and toxicity evaluation of amphiphilic metal complexes. (**a**) The library of amphiphilic metal complexes includes five kinds of hydrophobic tails, two kinds of linkers, and three kinds of metal ions. (**b**) The cytotoxicity of the metal complexes (the linker is a) against HepG2 cells at 70% survival of 3T3 cells. (**c**) The cytotoxicity of the metal complexes (the linker is b) to HepG2 cells at 70% survival of 3T3 cells. (**d**) The size and zeta potential of 2aZn nanoparticles prepared through the film dispersion method. (**e**) TEM images of 2aZn nanoparticles (20 μM). (**f**) Cytotoxicity of 2aZn in various cell lines

routes shown in Scheme S1). Many studies have shown that the DPA group chelated with metal ions has a high affinity for PS [29, 32–34]. Therefore, the hydrophilic heads of these molecules can effectively recognize PS on tumor cell membranes, and conjugation with a rationally designed hydrophobic tail enables selective disruption of the membrane. Next, we studied the cellular efficacy of these complexes. We initially assessed their cytotoxicity in normal 3T3 cells. To evaluate their antitumor activity and selectivity, we subsequently measured their cytotoxic effects on hepatocellular carcinoma HepG2 cells at concentrations that maintained 70% viability in 3T3 cells. As shown in Fig. 2b and c, when the linkers of these amphiphilic molecules were a, 2aZn treatment induced the most tumor cell death while preserving 3T3 cell viability (70%), indicating that 2aZn exhibited optimal antitumor efficacy and selectivity. When the linker was b, a Ni^{2+}-cordinated compound, 1bNi, showed the highest selectivity compared with the other compounds. Overall, 2aZn and 1bNi exhibit promising potential for selective tumor cell elimination. Given that Zn is a prevalent

element in the human body, we further investigated the anticancer properties of 2aZn in detail.

The increasing number of functional nanoparticles highlights the impressive versatility and preclinical potential of nanomedicine in cancer treatment [35–37]. Compared with traditional chemotherapy drugs, nanomedicine has fewer side effects and better pharmacokinetic activity [38–40]. However, it is only valid when the nanoparticle is stable in a complex physiological environment. Therefore, the development of a simple and stable nanomedicine is urgently needed [41]. Because of the amphiphilicity of 2aZn, it can form stable and uniform nanoparticles without any carriers. The average size of 2aZn remained consistent at approximately 45 nm as the concentration increased from 20 μM to 80 μM (Fig. 2d). Since 2aZn contains metal ions, the zeta potential of 2aZn was highly positive even at a concentration of 20 μM, indicating that the nanomicelles formed from 2aZn are highly stable. The TEM results were consistent with the DLS results (Fig. 2e). Usually, PS is widely dispersed in various kinds of tumor outer cell membranes, so 2aZn should have a high cytotoxicity against many different types of tumor cells. The exposure of PS increases when cells die [42], which further strengthens the interaction of 2aZn with cell membranes. Through this self-accelerating mechanism, 2aZn can swiftly kill tumor cells. Hence, the anticancer activity of 2aZn was further examined in HeLa, U373, HepG2, and 4T1 cells. As expected, 2aZn could kill various tumor cells, and the majority of tumor cells were eradicated at 80 μM, while showing low cytotoxicity toward normal RAW 264.7 and 3T3 cells (Fig. 2f). Moreover, we compared the cytotoxicity and selectivity of 2aZn with those of oxaliplatin (L-OHP), which is one of the most widely used platinum-based anticancer drugs in the clinic [43]. As demonstrated in Fig. S17a, 2aZn was more efficient to kill tumor cells than oxaliplatin at the same amount of metal, and the cytotoxicity of 20 μM 2aZn was equal to that of 100 μM oxaliplatin in CT-26 cells. In this regard, zinc therapy based on 2aZn has a substantially greater atomic economy than platinum treatment does. Importantly, unlike the toxic heavy metal platinum, zinc is abundant in the human body and is friendlier to the human body. Moreover, the cytotoxicity of 2aZn to normal 293T cells was significantly lower than that of oxaliplatin, suggesting that 2aZn is more selective than oxaliplatin (Fig. S17b). Furthermore, to study blood compatibility, we evaluated the hemolysis of 2aZn, and the results indicated that the haemolytic effect of 2aZn is marginal compared with its toxicity to tumor cells (Fig. S18).

Since 2aZn is a cationic amphiphilic metal complex, to ascertain whether it induces cell death through a mechanism involving cell membrane disruption, as illustrated in Fig. 3a, we next used SEM and TEM to investigate cell membrane morphology after 2aZn treatment. The PBS-treated cells were observed to have smooth and intact membranes, whereas after treatment with 2aZn, cell debris and pores in the membranes were found, and cell membrane integrity was disrupted (Fig. 3b and Fig. S19). The rupture of the cell membrane results in the loss of membrane functionality, ultimately leading to cell death [16]. To validate this mechanism, calcein/PI live–dead staining was used to evaluate cell membrane damage and cell death. As shown in Fig. 3c, compared with that in the PBS group, PI fluorescence was observed at a low concentration of 2aZn (5.0 μM), demonstrating that 2aZn could damage the tumor cell membrane, causing cell death, and that PI thus entered the cell. Additionally, we evaluated the degree of cell death induced by 2aZn via an Annexin V-FITC/PI dual-staining assay. The results revealed that 50.5% of the tumor cells treated with 2aZn (30 μM) experienced membrane rupture-mediated death, as evidenced by simultaneous staining with Annexin V-FITC and PI (Fig. 3d), indicating its potent antitumor activity. It has been reported that damage to the cell membrane causes the intracellular contents, such as ATP and lactate dehydrogenase (LDH), to flow out [44]. Therefore, we further evaluated the extracellular ATP and LDH concentrations after 2aZn treatment. As shown in Fig. 3e, at 5.0 μM, 2aZn increased extracellular ATP by 50% within 4 h, while higher concentrations paradoxically reduced ATP levels, likely due to rapid cell death limiting ATP production. Similarly, the LDH test results revealed that treatment with 2aZn could induce LDH leakage (Fig. 3f). Overall, these results demonstrated that 2aZn triggers tumor cell death via membrane disruption.

Cell membranes contain diverse phospholipids [45], including phosphatidylcholine (PC), phosphatidylethanolamine (PE), and PS. Given the high affinity of DPA-Zn to PS on the tumor cell membrane, we investigated whether the membrane-disruptive activity of 2aZn depends on PS recognition. We prepared PC/PE and PC/PE/PS liposomes to mimic cell membranes and encapsulated carboxyfluorescein (CF) within them. CF exhibits aggregation-induced quenching when it aggregates inside liposomes but regains fluorescence upon leakage into the surrounding medium [46]. Figure 4a showed that when PS was absent in liposomes, negligible fluorescence of CF was detected following incubation with 20 μM 2aZn. In contrast, PS-containing liposomes exhibited a time-dependent increase in fluorescence upon 2aZn (20 μM) treatment, with 20% CF released within 20 min (Fig. 4b), confirming the PS-dependent membrane disruption of 2aZn. We further evaluated the zeta potential of the liposomes to study the PS-targeting ability of 2aZn. 2aZn treatment hardly changed the zeta potential of the PC/PE liposomes (Fig. 4c). In contrast, PS-containing liposomes exhibited a significant shift from − 34.5 mV

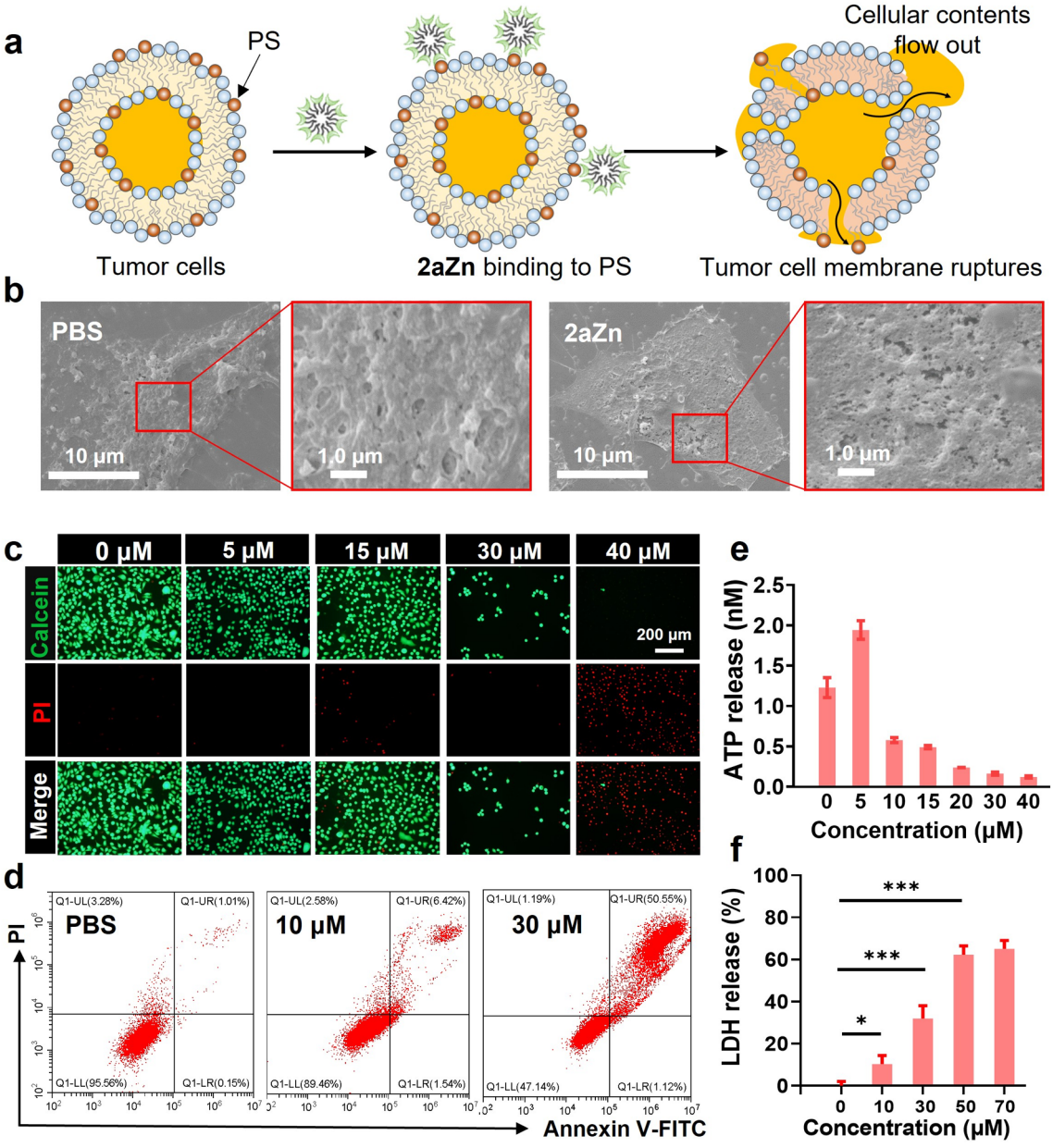

Fig. 3 Characterization of cell membrane disruption by 2aZn. (**a**) Schematic illustration of 2aZn specifically binding to PS on the outer leaflet of the tumor cell membrane, leading to tumor cell membrane disruption. (**b**) SEM images of the tumor cell membranes after treatment with 2aZn. (**c**) Fluorescence images of calcein-AM and PI double-stained tumor cells after treatment with different concentrations of 2aZn. (**d**) Flow cytometric analysis results of the Annexin V-FITC/PI staining of tumor cells treated with different concentrations of 2aZn. (**e**) Extracellular ATP content of tumor cells after treatment with various concentrations of 2aZn. (**f**) LDH release by tumor cells after treatment with various concentrations of 2aZn

to −17.5 mV posttreatment, finally matching the zeta potential of PC/PE liposomes, indicating that 2aZn could selectively interact with PS to perturb PS-containing liposomes. TEM analysis revealed that 2aZn selectively disrupted PS-containing (PC/PE/PS) liposomes, whereas PC/PE liposomes retained structural integrity (Fig. 4d). In addition, we generated PC/PE/PS giant vesicles and observed the morphological changes triggered by 2aZn via confocal laser scanning microscopy. All the vesicles were labelled with FM4-64 dye (red fluorescence), while PS was specifically labelled with Annexin V-FITC (green fluorescence). As depicted in Fig. 4e, before 2aZn treatment, the PC/PE/PS giant vesicles exhibited a typical spherical morphology. However, after 2aZn treatment, their form became irregular. Compared with that of the untreated vesicles, the surface of the unruptured vesicles treated with 10 μM 2aZn contained less PS labelled with Annexin V-FITC. When the samples were treated with

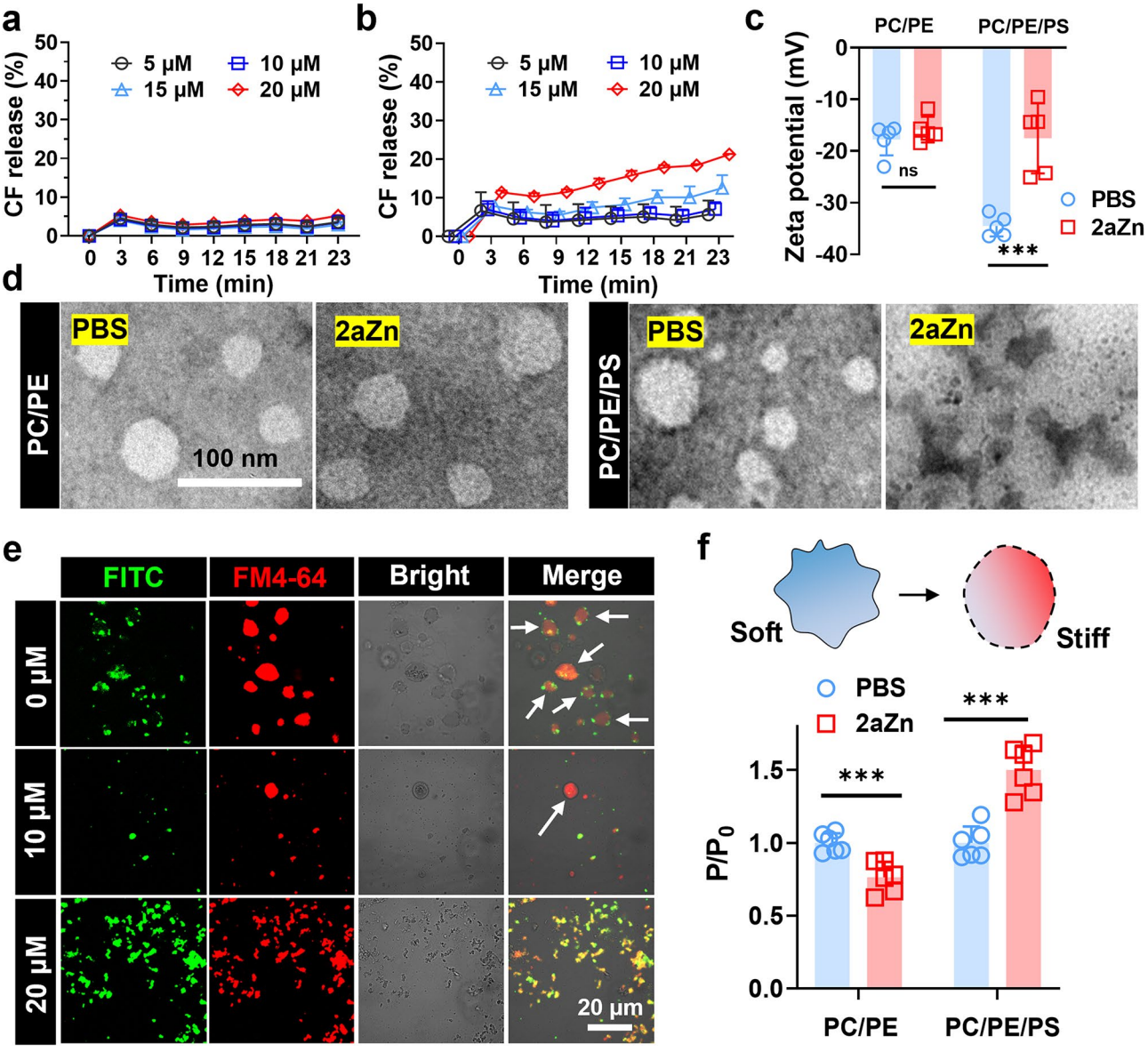

Fig. 4 Evaluation of the selective membrane-disrupting effect of 2aZn using liposomes with different compositions. (**a**) Evaluation of leakage from PC/PE liposomes treated with 2aZn by monitoring the fluorescence intensity of the released 5-carboxyfluorescein. (**b**) Assessment of leakage from PC/PE/PS liposomes treated with 2aZn by monitoring the fluorescence intensity of the released 5-carboxyfluorescein. (**c**) Changes in the zeta potential of the liposomes after treatment with 2aZn (20 μM). (**d**) TEM images of liposomes before and after treatment with 2aZn (20 μM). (**e**) Confocal laser scanning microscopy images of PC/PE/PS giant vesicles after treatment with different concentrations of 2aZn. PS was stained with annexin V-FITC (green), and giant vesicles were stained with FM4-64 (red). (**f**) Fluorescence polarization of liposomes before (P_0) and after treatment (P) with 2aZn (20 μM)

20 μM 2aZn, numerous fragments were observed, with a significant amount of PS labeled with Annexin V-FITC appearing in these fragments. These results suggested that 2aZn can alter the surface properties of PS-containing vesicles and induce lipid redistribution. Owing to the fluidity of the lipid bilayer in cell membranes, cells can deform to complete various physiological activities [47], which also plays an important role in tumor metastasis [48]. Given the change in the surface properties of PS-containing liposomes after 2aZn treatment, we further investigated the fluidity change after 2aZn treatment by measuring the fluorescence polarization (FP) of TMA-DPH, which is a probe that is highly sensitive to the repositioning caused by changes in the surrounding lipids and is commonly used to detect the fluidity of cell membranes [49, 50]. The results revealed that 2aZn treatment decreased the fluidity of the PS-containing liposomes, which may result from membrane disturbance and damage induced by 2aZn (Fig. 4f). Therefore, 2aZn could not only change the zeta potential of liposomes and destroy their morphology but also reduce their fluidity. The obtained data showed that 2aZn could effectively

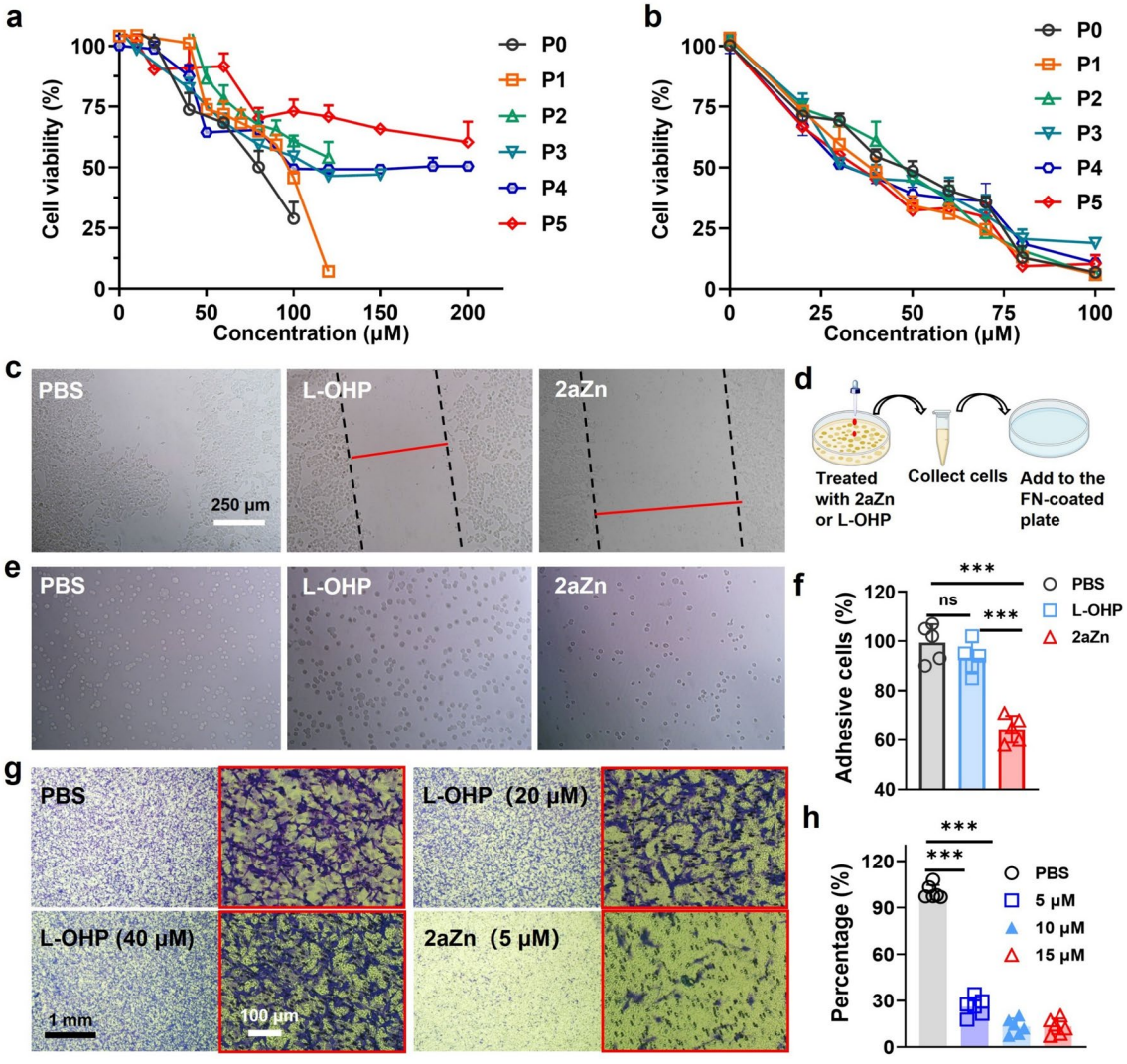

Fig. 5 Evaluation of drug resistance development and antitumour metastasis activity in vitro. (**a**) Development of oxaliplatin resistance in HepG2 cells. (**b**) Development of drug resistance to 2aZn in HepG2 cells. (**c**) Representative images of wound-healing assays in HepG2 cells subjected to different treatments. (**d**) Scheme of the cell adhesion experiment. (**e**) Representative images of tumor cells adhered to the FN-coated plates after different treatments. (**f**) The percentage of tumor cells that adhered to the FN-coated plates after different treatments. (**g**) Representative images of the transwell assay results for each group. (**h**) Percentage of tumor cells that passed through the matrix and filter of the transwell after being treated with different concentrations of 2aZn

recognize PS in liposomes and selectively change the properties of PS-containing liposomes.

The majority of cancer patients are resistant to chemotherapy drugs and suffer from significant tumor metastasis, which is the leading cause of mortality [51, 52]. How to avoid drug resistance and tumor metastasis is a major issue in the late period of tumor treatment [53, 54]. Previous research has suggested that the intact tumor cell membranes facilitates the efflux of drugs from cells, thereby contributing to drug resistance [55]. Furthermore, because metastatic cells are generally softer than their nonmalignant counterparts, high deformability is thought to confer a significant advantage in terms of metastatic potential [56]. Therefore, the intact function of tumor cell membranes is the basis of drug resistance and metastasis. Given that 2aZn can target tumor cell membranes through interactions with PS and damage the constructed liposomes, reducing their fluidity, the ability of 2aZn to overcome drug resistance and combat tumor metastasis is highly desirable. As shown in Fig. 5a, the sensitivity of HepG2 cells to oxaliplatin was considerably reduced after periods of stimulation. Specifically, almost all the primary cells (P0) died at 100 μM oxaliplatin, while most of the 5 generations of cells (P5) survived (75% survival) after treatment with 100 μM oxaliplatin. In the case of 2aZn, no alteration in drug sensitivity was observed in HepG2 cells following multiple treatments (Fig. 5b). Furthermore, at a concentration of 75 μM, the majority

of the cells died, a response similar to that observed in the initial state. Unlike traditional antitumor drugs, 2aZn kills tumor cells by destroying cell membranes, which makes the cell unable to develop drug resistance. Thus, 2aZn will not develop drug resistance after long-term treatment. On the other hand, the cell membrane is the main barrier that restricts drug entry, making it difficult for drugs to enter cells and penetrate solid tumors, thus leading to the development of drug resistance. As shown in Fig. S20, treatment with DOX alone was ineffective for DOX-resistant MCF-7/ADR cells. However, after co-incubation with 2aZn, the cytotoxicity of DOX significantly increased, effectively killing MCF-7/ADR cells, which was attributed to the increase in the intracellular DOX content following disruption of the cell membranes by 2aZn. Furthermore, we evaluated the ability of 2aZn to penetrate tumor tissue via a 3D tumor cell spheroid model. As shown in Fig. S21, free DOX had a limited ability to penetrate cell spheroids, whereas after treatment with 2aZn, the depth of penetration of DOX in the cell spheroids increased. These results demonstrated that 2aZn disrupted the barrier of the cell membrane.

The cell membrane plays a key role in tumor growth and metastasis [57]. In the late stage of cancer, an increase in the negatively charged PS content in the tumor cell membrane leads to increased electrostatic repulsion between the tumor cells, and the tumor cells readily fall off and metastasize. The elevation of PS levels enhances the interaction between exfoliated tumor cells and the stroma, thereby facilitating the formation of new metastases. Since our experiments revealed that 2aZn could increase the zeta potential while decrease the fluidity of PS-containing liposomes, 2aZn may have the potential to inhibit the metastasis of tumor cells. After 48 h of incubation, the cells in the PBS group clearly invaded, and the border line became indistinct, as shown in Fig. 5c. Compared with the oxaliplatin group, the 2aZn group presented larger voids, indicating that 2aZn was more effective than oxaliplatin in preventing tumor cell metastasis. When cells enter blood vessels, effective cell adhesion can promote the implantation of metastatic tumors, resulting in distal tumors. PS exposure is associated with increased cellular adhesion to endothelia [58]. Since PS is the main charged phospholipid in the tumor cell membrane, PS dominates the interaction with proteins through electrostatic interactions. When PS is caged with 2aZn, its interaction with fibronectin (FN) weakens to reduce the adhesion activity of the tumor. We performed a cell adhesion experiment to investigate the antiadhesion activity of 2aZn. As shown in Fig. 5d, after treatment with 2aZn, the cells were collected and added to FN-coated 96-well plates, and the adherent cells were counted. There were significantly fewer adherent cells in the 2aZn group than in the PBS group, with only 65% of the cells adhering to the FN-coated plates (Fig. 5e and f). Interestingly, there was no discernible difference between the oxaliplatin and PBS groups, indicating that oxaliplatin could hardly inhibit cell adhesion during tumor metastasis. Furthermore, the transwell assay results also demonstrated that 2aZn could effectively combat tumor metastasis (Fig. 5g). Even at low concentrations (5.0 μM), 2aZn could successfully prevent cells from passing through the matrix and filtering (75% of the cells lost invasion ability, Fig. 5h). However, even at 40 μM, oxaliplatin had no significant antitumor effect on metastasis. These results could be explained by the fact that a low dose of 2aZn could damage the cell membrane, reducing its deformability and resulting in the failure of cell invasion. In summary, 2aZn not only inhibited tumor cell invasion but also significantly reduced tumor cell adhesion to the extracellular matrix, thereby decreasing the possibility of tumor cell implantation at distant sites. Therefore, 2aZn has robust potential in combating tumor metastasis.

The in vivo antitumor activity of 2aZn was subsequently evaluated in an orthotopic 4T1 tumor-bearing mouse model. Before in vivo tumor treatment, we evaluated the in vivo distribution of 2aZn. As shown in Fig. S22, after intravenous injection of 2aZn, the zinc content in mouse tumor tissue significantly increased, demonstrating that 2aZn effectively accumulated at the tumor site. Next, we conducted an acute toxicity experiment with 2aZn in healthy mice to determine the therapeutic dose in these mice. As shown in Fig. S23a-d, intravenous administration of 2aZn at 40 mg/kg caused no mortality, significant weight loss, or tissue damage (H&E staining), with hematological parameters remaining normal, indicating its high biosafety. As shown in Fig. 6a, the tumor-bearing mice were treated with PBS, oxaliplatin (10 mg/kg), or 2aZn (10 mg/kg) via intratumoral injection every other day for a total of three times. During the treatment, the body weights and tumor volumes of the mice were recorded every other day. The body weights of the mice in all the groups did not decrease, indicating that 2aZn had no systemic toxicity (Fig. 6b). As shown in Fig. 6c-e, the tumors in the PBS group exhibited an increased growth rate, and 2aZn inhibited the tumor growth efficiently. Specifically, at the end of the treatment, the average tumor volume in the PBS group was 15 times greater than the initial volume, and the average tumor volume in the oxaliplatin group was 5 times greater than the initial volume. In contrast, the tumor volume and tumor weight of the 2aZn group were the smallest among all the groups throughout the entire treatment period. Compared with those of the PBS group, the tumor inhibition rate of the 2aZn group was as high as 93.4%. The major organs, including the heart, liver, spleen, lung, and kidney, were separated after treatment. The spleens in the 2aZn group

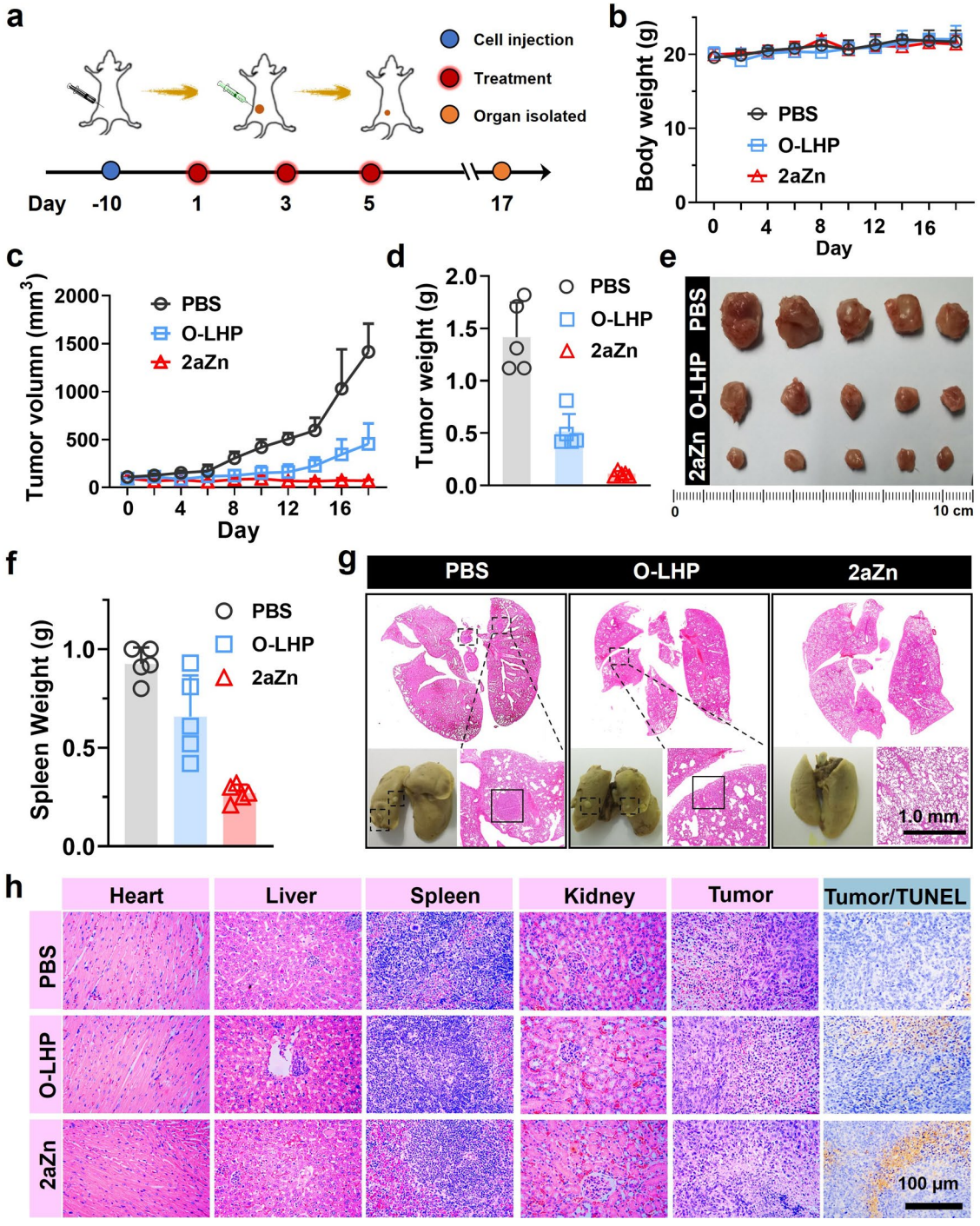

Fig. 6 Evaluation of antitumour activity using orthotopic tumor models constructed with 4T1 cells. (**a**) Schematic illustration of the experimental process. (**b**) The body weights of the mice during the treatment. (**c**) Tumor volume during treatment. (**d**) Tumor weight and (**e**) tumor images at the end of treatment. (**f**) Spleen weight at the end of treatment. (**g**) H&E staining of lung tissue. (**h**) H&E staining results for major tissues and TUNEL staining results for tumor tissues

were much smaller than those in the PBS group, whose average weight was only 27% that of the PBS group (Fig. 6f and Fig. S24). It is possible that 2aZn effectively inhibited tumor growth, resulting in fewer inflammatory cells in the 2aZn group than in the PBS and oxaliplatin groups [59]. At the end of treatment on day 17, hematoxylin and eosin (H&E) staining revealed that tumor cells metastasized to the lungs in the PBS and oxaliplatin groups (Fig. 6g). In contrast, the alveolar tissue was very regular, and there was no obvious inflammatory cell

infiltration or metastatic tumors in the 2aZn group, demonstrating its antimetastatic activity in vivo. Moreover, H&E staining of the major tissues and TUNEL staining of the orthotopic breast tumors revealed no pathological abnormalities in the major organs of the 2aZn group, indicating that there was no systematic toxicity and that there were more necrotic cells in the tumors of this group (Fig. 6h). Taken together, these findings suggest that 2aZn is a safe and highly potent antitumor drug with tumor-targeting and metastasis-suppressing activities.

Considering the potential of 2aZn in combating metastasis, we established a metastatic model via intravenous injection of Luc-4T1 cells into BALB/c mice to further study the antimetastatic activity of 2aZn in vivo. As shown in Fig. 7a, Luc-4T1 cells were intravenously injected into the mice, and the mice were subsequently divided randomly into three groups. On the 1st, 3rd, and 5th days, the mice in each group received PBS, oxaliplatin (100 μL, 2.5 mg/mL), or 2aZn (100 μL, 2.5 mg/mL) via tail vein injection. Tumor progression was monitored via an IVIS Spectrum imaging system on the 3rd, 6th, 12th, and 21st days after D-luciferin injection. As shown in Fig. 7b, the PBS and oxaliplatin groups displayed bright fluorescence during the treatment phase, indicating successful metastasis of the tumor cells to the lung. In contrast, 2aZn treatment markedly attenuated tumor cell dissemination, with minimal pulmonary colonization observed at the end of treatment. Notably, during treatment, oxaliplatin caused significant body weight loss, indicating that oxaliplatin has systemic toxicity (Fig. 7c). In contrast, there was no significant difference in body weight between the 2aZn and PBS groups, demonstrating the excellent biocompatibility of 2aZn. Survival analysis revealed 50% mortality within 21 days in the PBS and oxaliplatin groups due to the metastatic burden, whereas all 2aZn-treated mice survived (Fig. 7d). On day 22, the mice were euthanized, and the main organs were excised. The H&E staining results of the heart, liver, spleen, and kidney in all groups revealed no pathological changes (Fig. S25). Owing to excessive tumor growth, the lung weight in the PBS group increased significantly, and the average lung weight in the PBS group was 0.64 g, which was 2.3-fold greater than that in the 2aZn treatment group (0.28 g), indicating the substantial inhibitory effect of 2aZn on tumor metastasis (Fig. 7e). Furthermore, the images and H&E staining of lung tissue revealed that a considerable number of metastatic lesions could be observed in the PBS and oxaliplatin groups (Fig. 7f), which was the reason for the death of the mice, indicating that traditional chemotherapy fails to treat tumor metastasis. Overall, 2aZn strongly inhibited lung metastasis in vivo.

Conclusion

In summary, we constructed a library of amphiphilic complexes utilizing DPA-M^{2+} (M is Zn, Co, or Ni) as the hydrophilic head group. Through screening, we identified a zinc complex, denoted 2aZn, which exhibits high tumor selectivity, low hemolytic activity, and broad-spectrum antitumour efficacy. Mechanistic studies revealed that 2aZn specifically recognizes PS on the outer leaflet of tumor cell membranes, disrupting membrane stability through interactions with the lipid bilayer and ultimately leading to membrane rupture and tumor cell death. Notably, by targeting membrane lipids, a site with low mutational potential, 2aZn does not induce drug resistance under prolonged treatment. Furthermore, damaged membranes exhibit increased rigidity and reduced adhesion, effectively inhibiting tumor cell metastasis. As an amphiphilic molecule, 2aZn self-assembles into nanoparticles and achieves efficient accumulation in tumor tissues in vivo through a dual-targeting mechanism that combines PS recognition on tumor cell membranes with the enhanced permeability and retention (EPR) effect. The 3D tumor spheroid model further confirmed its superior tissue-penetrating ability. In vivo experiments demonstrated that 2aZn markedly suppressed tumor growth and blocked metastasis without inducing systemic toxicity.

Despite these advances, the structures of these compounds require further optimization to increase their efficacy and safety. We have designed and synthesized a library of dozens of metal complexes for screening. Future work will integrate computer-aided drug design and artificial intelligence-driven high-throughput screening to improve efficiency [60, 61]. Additionally, the current research is only limited to small animal models and lacks validation in large mammalian models or clinical trials. Future studies should evaluate the therapeutic efficacy and long-term safety of 2aZn in larger mammalian models to establish a foundation for translational medical applications. Meanwhile, although PS is exposed to the outer leaflets of the plasma membrane of many tumor cells, PS of the cells at the site of inflammation is also externalized. Overall, this study integrates metal complexes with PS-targeting and membrane-lytic properties,

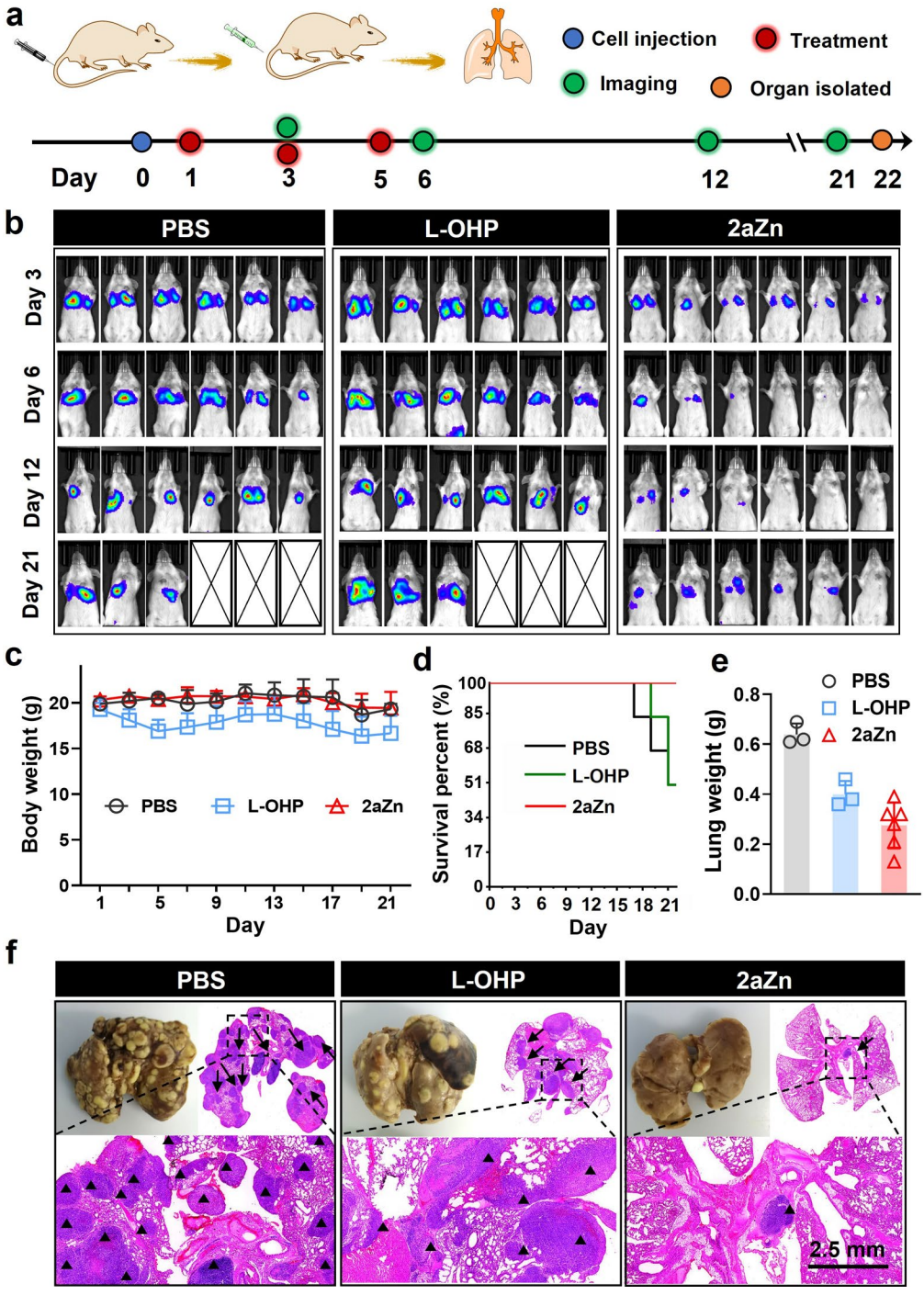

Fig. 7 Evaluation of the in vivo antimetastatic activity of 2aZn in a Luc-4T1 cell metastasis model. (**a**) Schematic illustration of the experimental process. (**b**) In vivo bioluminescence imaging at predetermined intervals during the experiment. (**c**) Body weight of mice during the treatment. (**d**) Percent survival of the mice in each group during the treatment. (**e**) The average weight of the lung tissue in each group at the end of treatment. (**f**) Images and H&E staining of lung tissue

establishing a novel anticancer strategy that achieves high efficacy, drug resistance avoidance, and metastasis suppression through specific disruption of tumor cell membranes, thereby providing a new paradigm for anti-tumour drug design.

Supplementary Information

The online version contains supplementary material available at https://doi.org/10.1186/s12951-025-03418-7.

Supplementary Material 1

Acknowledgements
Not applicable.

Author contributions
XH. Zhou: Writing-original draft, methodology. JW. Wang: Methodology, conceptualization. W. You, F. Gao, Z. Wang, JG Hong: Methodology, formal analysis. AZ. Shen: Methodology. YH. Ou: Methodology, formal analysis. Z. Xiang, LQ Tang: Methodology, formal analysis. X. Nie: Writing-review & editing, conceptualization. YZ. You: Conceptualization, project administration, funding acquisition. All the authors have read and approved the content of the manuscript.

Funding
This work was financially supported by National Key R&D Program of China (2024YFB3814600), the National Natural Science Foundation of China (52131305, 52203196, 52273308), the Scientific Research Project of the Health Commission of Anhui Province (AHWJ2024Aa30476, AHWJ2024BAh30020), the Scientific Research Project of Anhui Provincial Education Department (2022AH040184, 2024AH010035), and the Anhui University Research Plan (2023AH053392).

Data availability
No datasets were generated or analysed during the current study.

Declarations

Ethics approval and consent to participate
All animal experiments were approved by the Institutional Ethical Committee of the University of Science and Technology of China USTCACUC23030122089.

Competing interests
The authors declare no competing interests.

Author details
[1]Department of Pharmacy, The First Affiliated Hospital of USTC, Division of Life Sciences and Medicine, University of Science and Technology of China, Hefei, Anhui 230001, China
[2]Department of Vascular Surgery, The First Affiliated Hospital of Anhui Medical University, Hefei, Anhui 230022, China
[3]Center for Reproduction and Genetics, The First Affiliated Hospital of USTC, Division of Life Sciences and Medicine, University of Science and Technology of China, Hefei, Anhui 230001, China
[4]Key Laboratory of Precision and Intelligent Chemistry and Hefei National Laboratory for Physical Sciences at Microscale, University of Science and Technology of China, Hefei 230026, China
[5]Department of Gastroenterology, The Second Affiliated Hospital of Anhui Province, Hefei, Anhui 230601, China
[6]Anhui Provincial Key Laboratory of Precision Pharmaceutical Preparations and Clinical Pharmacy, Hefei, Anhui 230001, China

Received: 6 January 2025 / Accepted: 27 April 2025
Published online: 20 May 2025

References

1. Demaria O, Cornen S, Daron M, Morel Y, Medzhitov R, Vivier E. Harnessing innate immunity in cancer therapy. Nature. 2019;574:45–56.
2. Shi J, Kantoff PW, Wooster R, Farokhzad OC. Cancer nanomedicine: progress, challenges and opportunities. Nat Rev Cancer. 2017;17:20–37.
3. Rosenblum D, Joshi N, Tao W, Karp JM, Peer D. Progress and challenges towards targeted delivery of cancer therapeutics. Nat Commun. 2018;9:1410.
4. Mitchell MJ, Jain RK, Langer R. Engineering and physical sciences in oncology: challenges and opportunities. Nat Rev Cancer. 2017;17:659–75.
5. Grosset JH. The new challenges for chemotherapy research. Lepr Rev. 2000;71:100–4.
6. Minchinton AI, Tannock IF. Drug penetration in solid tumours. Nat Rev Cancer. 2006;6:583–92.
7. Tannock IF, Lee C, Tunggal JK, Cowan DS, Egorin MJ. Limited penetration of anticancer drugs through tumor tissue: a potential cause of resistance of solid tumors to chemotherapy. Clin Cancer Res. 2002;8:878–84.
8. Lin KH, Rutter J, Xie A, Pardieu B, Winn ET, Dal Bello R, et al. Using antagonistic Pleiotropy to design a chemotherapy-induced evolutionary trap to target drug resistance in cancer. Nat Genet. 2020;52:408–17.
9. Sun T, Zhang YS, Pang B, Hyun DC, Yang M, Xia Y. Engineered nanoparticles for drug delivery in Cancer therapy. Angew Chem Int Ed. 2014;53:12320–64.
10. Chauhan VP, Jain RK. Strategies for advancing cancer nanomedicine. Nat Mater. 2013;12:958–62.
11. Lammers T, Kiessling F, Ashford M, Hennink WE, Crommelin DJA, Storm G. Cancer nanomedicine: is targeting our target? Nat Rev Mater. 2016;1:16069.
12. Akinc A, Maier M, Manoharan M, Fitzgerald K, Jayaraman M, Barros S, et al. The Onpattro story and the clinical translation of nanomedicines containing nucleic acid-based drugs. Nat Nanotechnol. 2019;14:1084–87.
13. Liao Y-S, Liang J-X, Wen Z, Cai M-Z, Song Z-Z, Zhang N-Y, et al. Strategies and applications of cell membrane surface functionalization of polymer materials. Acta Polym Sin. 2024;55:553–72.
14. Blanco E, Shen H, Ferrari M. Principles of nanoparticle design for overcoming biological barriers to drug delivery. Nat Biotechnol. 2015;33:941–51.
15. Hillaireau H, Couvreur P. Nanocarriers' entry into the cell: relevance to drug delivery. Cell Mol Life Sci. 2009;66:2873–96.
16. Stewart MP, Langer R, Jensen KF. Intracellular delivery by membrane disruption: mechanisms, strategies, and concepts. Chem Rev. 2018;118:7409–531.
17. Shao N, Yuan L, Liu L, Cong Z, Wang J, Wu Y, Liu R. Reversing anticancer drug resistance by synergistic combination of chemotherapeutics and membranolytic antitumor β-peptide polymer. J Am Chem Soc. 2024;146:11254–65.
18. Shao N, Yuan L, Ma P, Zhou M, Xiao X, Cong Z, et al. Heterochiral β-peptide polymers combating multidrug-resistant cancers effectively without inducing drug resistance. J Am Chem Soc. 2022;144:7283–94.
19. Park NH, Cheng W, Lai F, Yang C, Florez de Sessions P, Periaswamy B, et al. Addressing drug resistance in cancer with macromolecular chemotherapeutic agents. J Am Chem Soc. 2018;140:4244–52.
20. Shen W, Zhang Y, Wan P, An L, Zhang P, Xiao C, Chen X. Antineoplastic Drug-Free anticancer strategy enabled by Host-Defense-Peptides-Mimicking synthetic polypeptides. Adv Mater. 2020;32:2001108.
21. Liu M, Huang L, Zhang W, Wang X, Geng Y, Zhang Y, et al. A transistor-like pH-sensitive nanodetergent for selective cancer therapy. Nat Nanotechnol. 2022;17:541–51.
22. Wang J, Yuan Y, Su C, Bao Y, Xu W, Yao Y, et al. pH-Ultrasensitive membranolytic polyesters with alternating sequence of ionizable and hydrophobic groups for selective oncolytic therapy. J Am Chem Soc. 2024;147:1008–16.
23. Fan F, Jin L, Yang L. pH-sensitive nanoparticles composed solely of membrane-disruptive macromolecules for treating pancreatic cancer. ACS Appl Mater Interfaces. 2021;13:12824–35.
24. Sharma B, Kanwar SS, Phosphatidylserine. A cancer cell targeting biomarker. Semin Cancer Biol. 2018;52:17–25.
25. Birge R, Boeltz S, Kumar S, Carlson J, Wanderley J, Calianese D, et al. Phosphatidylserine is a global immunosuppressive signal in efferocytosis, infectious disease, and cancer. Cell Death Differ. 2016;23:962–78.
26. Riedl S, Rinner B, Asslaber M, Schaider H, Walzer S, Novak A, et al. In search of a novel target—Phosphatidylserine exposed by non-apoptotic tumor cells and metastases of malignancies with poor treatment efficacy. BBA-Biomembranes. 2011;1808:2638–45.
27. DeRyckere D, Huelse JM, Earp HS, Graham DK. TAM family kinases as therapeutic targets at the interface of cancer and immunity. Nat Rev Clin Oncol. 2023;20:755–79.
28. Peng K, Zheng Y, Xia W, Mao Z-W. Organometallic anti-tumor agents: targeting from biomolecules to dynamic bioprocesses. Chem Soc Rev. 2023;52:2790–832.
29. Zwicker VE, Oliveira BL, Yeo JH, Fraser ST, Bernardes GJ, New EJ, Jolliffe KA. A fluorogenic probe for cell surface phosphatidylserine using an intramolecular indicator displacement sensing mechanism. Angew Chem Int Ed. 2019;58:3087–91.
30. Gao F, You W, Zhang L, Shen A-Z, Chen G, Zhang Z, et al. Copper chelate targeting externalized phosphatidylserine inhibits PD-L1 expression and enhances Cancer immunotherapy. J Am Chem Soc. 2025;147:5796–807.
31. Sharma VD, Ilies MA. Heterocyclic cationic gemini surfactants: A comparative overview of their synthesis, self-assembling, physicochemical, and biological properties. Med Res Rev. 2014;34:1–44.
32. Weng J, Wang Y, Zhang Y, Ye D. An activatable Near-Infrared fluorescence probe for in vivo imaging of acute kidney injury by targeting phosphatidylserine and Caspase-3. J Am Chem Soc. 2021;143:18294–304.
33. Shao Q, Shen C-L, You W, Nie X, Huang W-Q, Gao F, et al. DPA-Zn enables targeting and bypassing endosomal trapping delivery of a genome-editing

system into cancer cells via phosphatidylserine-mediated endocytic pathway. Chem Eng J. 2024;498:155596.
34. Nie X, You W, Zhang Z, Gao F, Zhou XH, Wang HL, et al. DPA-Zinc around polyplexes acts like PEG to reduce protein binding while targeting Cancer cells. Adv Healthc Mater. 2023;12:2203252.
35. Umer A, Ghouri MD, Muyizere T, Aqib RM, Muhaymin A, Cai R, Chen C. Engineered Nano–Bio interfaces for stem cell therapy. Precis Chem. 2023;1:341–56.
36. Huang W-Q, You W, Zhu Y-Q, Gao F, Wu Z-Z, Chen G, et al. Autophagosomes coated in situ with nanodots act as personalized cancer vaccines. Nat Nanotechnol. 2025;20:451–62.
37. Huang WQ, Zhu YQ, Gao F, You W, Chen G, Nie X, et al. Nanogalvanic cells release highly reactive electrons in tumors to effectively eliminate tumors. Adv Mater. 2024;36:2404199.
38. Der Meel RV, Sulheim E, Shi Y, Kiessling F, Mulder WJM, Lammers T. Smart cancer nanomedicine. Nat Nanotechnol. 2019;14:1007–17.
39. Lu GL, Jin YT, Liu XR, Huang CJ. Stimulus-responsive polymeric nanocarriers for platinum drug delivery. Polym Bull. 2024;37:1317–36.
40. Zhou M-X, Zhang J-Y, Cai X-M, Dou R, Ruan L-F, Yang W-J, et al. Tumor-penetrating and mitochondria-targeted drug delivery overcomes doxorubicin resistance in lung cancer. Chin J Polym Sci. 2023;41:525–37.
41. Nishiyama N. Nanocarriers shape up for long life. Nat Nanotechnol. 2007;2:203–04.
42. Vermes I, Haanen C, Steffensnakken H, Reutelingsperger CPM. A novel assay for apoptosis. Flow cytometric detection of phosphatidylserine expression on early apoptotic cells using fluorescein labelled Annexin V. J Immunol Methods. 1995;184:39–51.
43. Arena S, Corti G, Durinikova E, Montone M, Reilly NM, Russo M, et al. A subset of colorectal cancers with cross-sensitivity to Olaparib and oxaliplatin. Clin Cancer Res. 2020;26:1372–84.
44. Wiernicki B, Maschalidi S, Pinney J, Adjemian S, Vanden Berghe T, Ravichandran KS, Vandenabeele P. Cancer cells dying from ferroptosis impede dendritic cell-mediated anti-tumor immunity. Nat Commun. 2022;13:1–15.
45. Escribá PV, Busquets X, Inokuchi J, Balogh G, Török Z, Horváth I, et al. Membrane lipid therapy: modulation of the cell membrane composition and structure as a molecular base for drug discovery and new disease treatment. Prog Lipid Res. 2015;59:38–53.
46. Kenaan A, Cheng J, Qi D, Chen D, Cui D, Song J. Physicochemical analysis of DPPC and photopolymerizable liposomal binary mixture for Spatiotemporal drug release. Anal Chem. 2018;90:9487–94.
47. Doktorova M, Symons JL, Levental I. Structural and functional consequences of reversible lipid asymmetry in living membranes. Nat Chem Biol. 2020;16:1321–30.
48. Zhao W, Prijic S, Urban BC, Tisza MJ, Zuo Y, Li L, et al. Candidate antimetastasis drugs suppress the metastatic capacity of breast cancer cells by reducing membrane fluidity. Cancer Res. 2016;76:2037–49.
49. Sweedo A, Wise LM, Sheriff J, Bluestein D, Purdy JG, Slepian MJ. MCS hypershear modulates platelet membrane fluidity, lipid species, and is gender specific. J Heart Lung Transpl. 2020;39:S147.
50. do Canto AM, Robalo JR, Santos PD, Carvalho AJP, Ramalho JP, Loura LM. Diphenylhexatriene membrane probes DPH and TMA-DPH: A comparative molecular dynamics simulation study. BBA-Biomembranes. 2016;1858:2647–61.
51. Azmi AS, Bao B, Sarkar FH. Exosomes in Cancer development, metastasis and drug resistance: A comprehensive review. Cancer Metastasis Rev. 2013;32:623–42.
52. Park NH, Cheng W, Lai F, Yang C, De Sessions PF, Periaswamy B, et al. Addressing drug resistance in Cancer with macromolecular chemotherapeutic agents. J Am Chem Soc. 2018;140:4244–52.
53. Vasan N, Baselga J, Hyman DM. A view on drug resistance in cancer. Nature. 2019;575:299–309.
54. Martin OA, Anderson RL, Narayan K, Macmanus M. Does the mobilization of Circulating tumour cells during cancer therapy cause metastasis? Nat Rev Clin Oncol. 2017;14:32–44.
55. Peverelli E, Treppiedi D, Mangili F, Catalano R, Spada A, Mantovani G. Drug resistance in pituitary tumours: from cell membrane to intracellular signalling. Nat Rev Endocrinol. 2021;17:560–71.
56. Gensbittel V, Kräter M, Harlepp S, Busnelli I, Guck J, Goetz JG. Mechanical adaptability of tumor cells in metastasis. Dev Cell. 2021;56:164–79.
57. van der Meel R, Sulheim E, Shi Y, Kiessling F, Mulder WJM, Lammers T. Smart cancer nanomedicine. Nat Nanotechnol. 2019;14:1007–17.
58. Elliott JI, Surprenant A, Marelli-Berg FM, Cooper JC, Cassady-Cain RL, Wooding C, et al. Membrane phosphatidylserine distribution as a non-apoptotic signalling mechanism in lymphocytes. Nat Cell Biol. 2005;7:808–16.
59. Wan T, Pan Q, Ping Y. Microneedle-assisted genome editing: A transdermal strategy of targeting NLRP3 by CRISPR-Cas9 for synergistic therapy of inflammatory skin disorders. Sci Adv. 2021;7:eabe2888.
60. Luo Y. Chemistry in the era of artificial intelligence. Precis Chem. 2023;1:127–28.
61. Li Z. Artificial-Intelligence driven precision chemistry. Precis Chem. 2024;3:1–2.

Publisher's note